Measurement of the Higgs to invisible branching fraction at the FCC-ee

Andrew Mehta[1*], Stephen Randles[1*] and Nikolaos Rompotis[1*]

[1*]Oliver Lodge Laboratory, University of Liverpool, Oxford Road, Liverpool, L69 7ZE,UK.

*Corresponding author(s). E-mail(s): andrew.mehta@cern.ch; stephen.david.randles@cern.ch; nikolaos.rompotis@cern.ch;

The expected sensitivity, using statistical errors only, to the branching fraction of Higgs to invisible is given for the ZH process at the e^+e^- Future Circular Collider running at centre-of-mass energies of $\sqrt{s}$ = 240 GeV and $\sqrt{s}$ = 365 GeV with integrated luminosities of 10.8 ab^{-1} and 3 ab^{-1} respectively. The decays of the Z to electrons, muons, b-quarks, c-quarks and lighter quarks were investigated. It is found that a 25% measurement is possible if a Standard Model branching fraction of 0.106% for the process $H \to ZZ^* \to \nu\nu\nu\nu$ is assumed. The $Z \to qq$ channel has the best sensitivity. Additional new physics Higgs to invisible decays could be observed with a sensitivity of greater than 5σ if the branching fraction exceeds 0.13% or could be excluded at 0.052% at 95% confidence level.

1 Introduction

The Future Circular Collider (FCC) project is a proposed series of accelerators at CERN hosted in a planned tunnel with circumference 100 km in the Geneva area [1]. The first stage of FCC will include an electron-positron collider that is expected to run at centre-of-mass energies $\sqrt{s}$=240 GeV and 365 GeV. The run at $\sqrt{s}$ = 240 GeV is at the threshold to produce a Higgs boson, H in association with a Z boson ($e^+e^- \to ZH$) and will be dedicated to precision Higgs boson physics. The 365 GeV run, whose main objective is to make a detailed study of the top-quark, will also produce reasonable numbers of Higgs bosons.

An advantage of studying the Higgs boson in e^+e^- collisions through the ZH production is that because electrons are elementary particles and the centre-of-mass energy of the individual collisions is known, by identifying and measuring the decay products of the Z boson the mass of the system recoiling against it can be calculated using the formula:

$$M_{\text{rec}} = \sqrt{(\sqrt{s} - E_Z)^2 - \vec{p}_Z^{\,2}} \ ,$$

where E_Z and $\vec{p}_Z$ are the total energy and momentum of the Z boson system. This mass, M_{rec}, is referred to as the "recoil mass." The recoil mass distribution is expected to peak a the Higgs boson mass, i.e. around 125 GeV and therefore provides access to the Higgs boson without any need to reconstruct its decays. This allows the production and decay of the Higgs boson to be separated, leading eventually to an absolute measurement of the Higgs boson couplings. In the case of the Z recoiling against invisible particles M_{rec} equals the mass of the invisible particles m_{miss}. This opens the way for a clean measurement of the Higgs boson to invisible particles, which is much better than what can be achieved in any current hadron machine. In the Standard Model (SM), Higgs boson to invisible proceeds via the decay $H \to ZZ^* \to \nu\nu\nu\nu$ and has a branching ratio of 1.06×10^{-3} [2]. However, it is possible in the Higgs portal model that Higgs boson decays to non-SM invisible particles, possibly related to dark matter [3, 4] and this is a further motivation for studying this channel.

The current searches for Higgs boson to invisible particles come from ATLAS and CMS experiments at the LHC, which report an 95% confidence level upper limit of 10.7% [5] and 15% [6], respectively. These values are much larger than the expected value from the SM, which is not within the reach of the current LHC programme.

There have been several studies of the sensitivity to Higgs boson decays to invisible particles in future accelerators. A study for CepC, which is a Chinese proposal for an e^-e^+ machine, very similar to FCC-ee, reports an upper limit on the Higgs boson branching ratio of 0.26% by including only $Z \to ee$, $\mu\mu$ and bb [7]. A study for the FCC conceptual design report [1] quotes an upper limit of 0.3%. In other studies, e.g. in Ref. [8] an upper limit of about 0.6% is quoted by using $Z \to ee$ and $\mu\mu$ decays.

This study aims to estimate the sensitivity to Higgs boson to invisible particles using $e^+e^- \to ZH$ events in FCC-ee assuming $\sqrt{s} = 240$ GeV and $\sqrt{s} = 365$ GeV with integrated luminosities of 10.8 ab^{-1} and 3 ab^{-1} respectively. These luminosities are estimated for the scenario with the FCC running with four detectors. The study uses a simulation of the IDEA detector [9] using Delphes [10] processed with the official FCC software[1], using most of the visible decays of the Z boson: $Z \to ee$, $\mu\mu$, bb, cc and qq, where q denotes any of u, d or s. The different decays of the Z boson are treated as separate categories. The final result is extracted by fitting the m_{miss} distribution in each category.

2 Software framework and simulated samples

The samples that have been used are from the Winter2023 campaign accessed via:
`/eos/experiment/fcc/ee/generation/DelphesEvents/winter2023/IDEA/` .
The samples below refer to $\sqrt{s} = 240$ GeV and the integrated luminosity assumed is 10.8 ab^{-1}. The particular processes that have been considered along with their sample names are:

[1] `https://github.com/HEP-FCC/FCCAnalyses`

- Higgs boson production (with inclusive Higgs boson decays)
  - wzp6_ee_eeH_ecm240
    $e^+e^- \to ZH$ with $Z \to ee$, $\sigma = 0.0071611$ pb
  - wzp6_ee_mumuH_ecm240
    $e^+e^- \to ZH$ with $Z \to \mu\mu$, $\sigma = 0.0067643$ pb
  - wzp6_ee_nunuH_ecm240
    $e^+e^- \to ZH$ with $Z \to \nu\nu$, $\sigma = 0.046191$ pb
  - wzp6_ee_qqH_ecm240
    $e^+e^- \to ZH$ with $Z \to qq(u/d)$, $\sigma = 0.053337$ pb
  - wzp6_ee_tautauH_ecm240
    $e^+e^- \to ZH$ with $Z \to \tau\tau$, $\sigma = 0.0067518$ pb
- Higgs boson production (with Higgs bosson to ZZ*)
  - wzp6_ee_bbH_HZZ_ecm240
    $e^+e^- \to ZH$ with $Z \to bb$, $\sigma = 0.0007915$ pb
  - wzp6_ee_ccH_HZZ_ecm240
    $e^+e^- \to ZH$ with $Z \to cc$, $\sigma = 0.0006164$ pb
  - wzp6_ee_ssH_HZZ_ecm240
    $e^+e^- \to ZH$ with $Z \to ss$, $\sigma = 0.0007912$ pb
- Processes without a Higgs boson
  - p8_ee_WW_ecm240
    WW production, inclusive decays, $\sigma = 16.4385$ pb
  - p8_ee_ZZ_ecm240
    ZZ production, inclusive decays, $\sigma = 1.35899$ pb
  - p8_ee_Zqq_ecm240
    Z/γ^* production, hadronic decays only, $\sigma = 52.6539$ pb
  - wzp6_ee_ee_Mee_30_150_ecm240
    Z/γ^* production, ee channel, including t-channel exchange, only with $30 < m_{ee} < 150$ GeV and azimouthal angle $15° < \theta < 165°$, $\sigma = 8.305$ pb
  - wzp6_ee_mumu_ecm240
    Z/γ^* production, $\mu\mu$ channel, $\sigma = 5.288$ pb
  - wzp6_ee_tautau_ecm240
    Z/γ^* production, $\tau\tau$ channel, $\sigma = 4.668$ pb
  - wzp6_ee_nuenueZ_ecm240
    Z production via $\nu\nu$ fusion, W-exchange only, inclusive Z decays, $\sigma = 0.033274$ pb

The samples below refer to $\sqrt{s} = 365$ GeV and the integrated luminosity assumed is 3.0 ab^{-1}. The particular processes that have been considered along with their sample names are:

- Higgs boson production (with inclusive Higgs boson decays)
  - wzp6_ee_eeH_ecm365
    $e^+e^- \to ZH$ with $Z \to ee$, $\sigma = 0.00739$ pb
  - wzp6_ee_mumuH_ecm365

$e^+e^- \to ZH$ with $Z \to \mu\mu$, $\sigma = 0.004185$ pb

– wzp6_ee_nunuH_ecm365
  $e^+e^- \to ZH$ with $Z \to \nu\nu$, $\sigma = 0.05394$ pb
– wzp6_ee_qqH_ecm365
  $e^+e^- \to ZH$ with $Z \to qq(u/d)$, $\sigma = 0.0329977$ pb
– wzp6_ee_bbH_ecm365
  $e^+e^- \to ZH$ with $Z \to bb$, $\sigma = 0.018389$ pb
– wzp6_ee_ccH_ecm365
  $e^+e^- \to ZH$ with $Z \to cc$, $\sigma = 0.014436$ pb
– wzp6_ee_ssH_ecm365
  $e^+e^- \to ZH$ with $Z \to ss$, $\sigma = 0.018538$ pb
– wzp6_ee_tautauH_ecm365
  $e^+e^- \to ZH$ with $Z \to \tau\tau$, $\sigma = 0.004172$ pb

- Processes without a Higgs boson
  – p8_ee_WW_ecm365
    WW production, inclusive decays, $\sigma = 10.7165$ pb
  – p8_ee_ZZ_ecm365
    ZZ production, inclusive decays, $\sigma = 0.6428$ pb
  – p8_ee_Zqq_ecm365
    Z/γ^* production, hadronic decays only, $\sigma = 21.4149$ pb
  – wzp6_ee_ee_Mee_30_150_ecm365
    Z/γ^* production, ee channel, including t-channel γ exchange, only with $30 < m_{ee} < 150$ GeV and azimuthal angle $15° < \theta < 165°$, $\sigma = 1.527$ pb
  – wzp6_ee_mumu_ecm365
    Z/γ^* production, $\mu\mu$ channel, $\sigma = 2.2858$ pb
  – wzp6_ee_tautau_ecm365
    Z/γ^* production, $\tau\tau$ channel, $\sigma = 2.017$ pb
  – wzp6_ee_nuenueZ_ecm365
    Z production via $\nu\nu$ fusion, W-exchange only, inclusive Z decays, $\sigma = 0.12624$ pb
  – wzp6_ee_SM_tt_tlepThad_noCKMmix_keepPolInfo_ecm365
    tt production, top decay mixed leptonic and hadronic, $\sigma = 0.22$ pb
  – wzp6_ee_SM_tt_tlepTlep_noCKMmix_keepPolInfo_ecm365
    tt production, top decay fully leptonic, $\sigma = 0.106$ pb
  – wzp6_ee_SM_tt_thadTlep_noCKMmix_keepPolInfo_ecm365
    tt production, top decay mixed hadronic and leptonic, $\sigma = 0.22$ pb
  – wzp6_ee_SM_tt_thadThad_noCKMmix_keepPolInfo_ecm365
    tt production, top decay fully hadronic, $\sigma = 0.454$ pb

There are no dedicated samples for Higgs boson to $\nu\nu\nu\nu$ decays, which is the signal that is considered in this sensitivity study. The signal events are taken from the inclusive Higgs boson decays of the simulated samples that contain a Higgs boson mentioned before. The absence of a dedicated signal sample limits the available statistics of Higgs boson to invisible events in the final analysis.

The analysis of these samples has used the official FCC framework with `Key4HEP` release `key4hep-stack/2023-01-15` . This framework runs on these samples to perform some selection requirements and flavour tagging. Electrons and muons are used if they have $p_T > 10$ GeV. Jet clustering has been performed using anti-kT with the setup [11]:

```
JetClustering::clustering_ee_genkt(1.5, 0, 0, 0, 0, -1)
```

where the algorithm is running over all reconstructed particles. Flavour tagging of jet is performed using an FCC implementation of the ParticleNet algorithm [12, 13]. The algorithm provides identification of b, c, g or light-quark hadrons separately.

3 Analysis at $\sqrt{s} = 240$ GeV

The analysis considers channels, depending on the decay of the Z boson. Events cannot belong to more than one channel and the order of preference is as follows:

1. "ee" channel: exactly two electrons in the event;
2. "$\mu\mu$" channel: exactly two muons in the event;
3. "bb" channel: no electrons or muons in the event and at least one of the jets in the event is b-tagged (referred to in the following as b-jet) with a requirement that the ParticleNet output for b-jet tagging is greater than 0.9;
4. "cc" channel: no electrons or muons in the event and at least one of the jets in the event are c-tagged (referred to in the following as c-jet) with a requirement that the ParticleNet output for c-jet tagging is greater than 0.5;
5. "qq" channel: no electrons or muons in the event.

The cc channel is split into two sub-channels for one c-jet and ≥ 2 c-jets in order to better treat the $W \to cs$ background, which predominately occurs in the 1 c-jet sub-channel.

Events with only one or more than 2 electrons or muons are vetoed. In the hadronic channels events with a jet which has a ParticleNet output for a τ jet greater than 0.5 are vetoed. A requirement in the missing momentum, $p_{\mathrm{T}}^{\mathrm{miss}}$, of the event is imposed in order to suppress Z/γ^* background, which can have high energy photons that are lost down the beam pipe and thus little $p_{\mathrm{T}}^{\mathrm{miss}}$. This requirement is chosen to be $p_{\mathrm{T}}^{\mathrm{miss}} > 10$ GeV for the ee and $\mu\mu$ channels and $p_{\mathrm{T}}^{\mathrm{miss}} > 18$ GeV for the cc and bb channels, which have worse energy resolutions can be seen in Figure 1. The values for this selection and all others were chosen by applying the other analysis cuts in addition to the requirement $120 < m_{\mathrm{miss}} < 130$ GeV and choosing those values that improved the overall sensitivity defined by $S/\sqrt{(S+B)}$, where S (B) is the total number of signal (background) events. Some simplifications in the cuts were made, such as choosing rounded values and the same values for different categories, where there was negligible impact on the overall sensitivity.

The Z boson mass is reconstructed from the visible mass of all reconstructed particles, m_{vis}. This distribution is shown for signal and backgrounds in each channel in Figure 2. It can be seen that there is a large ZZ background where one Z decays to neutrinos and the other peaks at the Z mass. The WW background is large in the ee and $\mu\mu$ channels, where the major contribution is from decays where both Ws

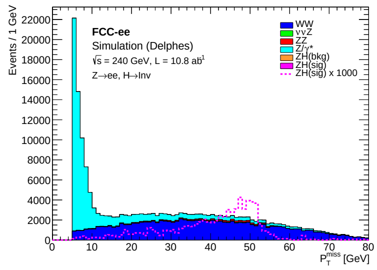

(a) ee channel

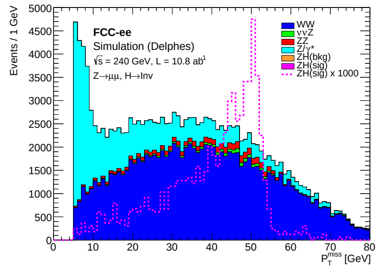

(b) $\mu\mu$ channel

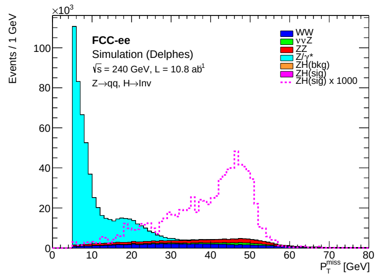

(c) qq channel

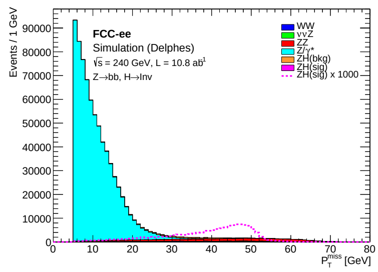

(d) bb channel

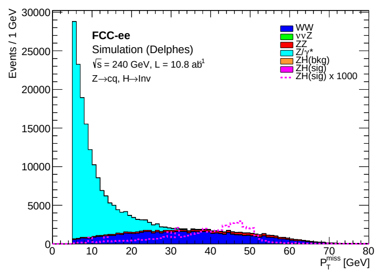

(e) cc channel, 1 c-jet

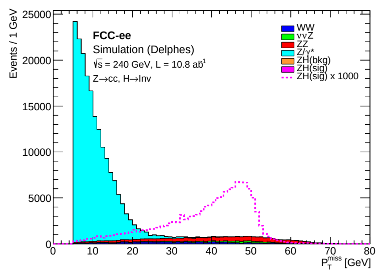

(f) cc channel, 2 c-jets

Fig. 1: The missing p_T distribution of the (a) ee, (b) $\mu\mu$, (c) qq, (d) bb and (e-f) cc channels for $\sqrt{s} = 240$ GeV after a requirement of $120 < m_{\text{miss}} < 130$ GeV. The cc channel has been split into two categories depending on the number of c-jets. For visual clarity events with $p_{\text{T}}^{\text{miss}} < 5$ GeV are removed and the signal is scaled by a factor of 100.

decay leptonically and in the qq and 1 c-jet cc channels where a mixture of one and two hadronic decays contribute. All channels have Z/γ^* background, which is largest in the cc and bb channels, due to heavy flavour decays with neutrinos that are not suppressed by the $p_{\text{T}}^{\text{miss}}$ cut. SM Higgs boson background is only significant in the bb channel due to the dominant $H \to bb$ decay but it is well separated in m_{vis} from the signal.

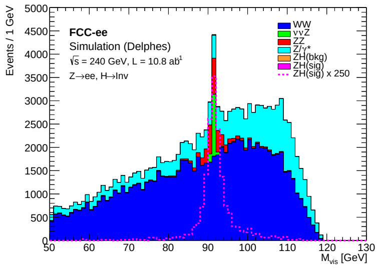

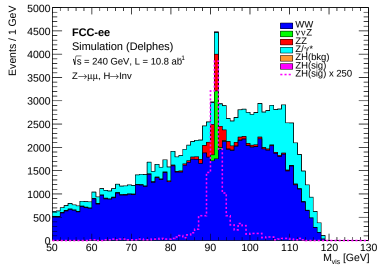

(a) ee channel

(b) $\mu\mu$ channel

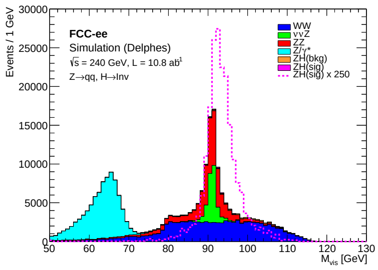

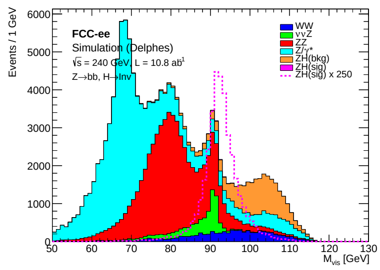

(c) qq channel

(d) bb channel

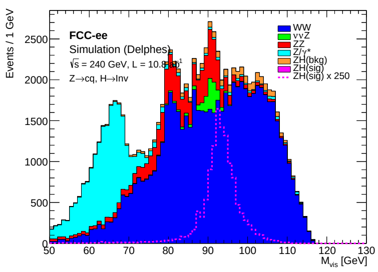

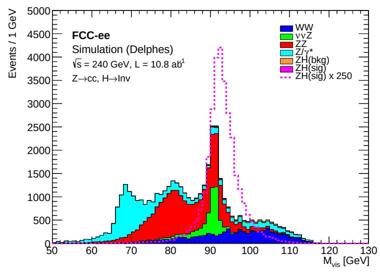

(e) cc channel, 1 c-jet

(f) cc channel, 2 c-jets

Fig. 2: The m_{vis} distribution of (a) ee, (b) $\mu\mu$, (c) qq, (d) bb and (e-f) cc channels for $\sqrt{s} = 240$ GeV after the $p_{\text{T}}^{\text{miss}}$ requirement and the additional requirement of $120 < m_{\text{miss}} < 130$ GeV. The cc channel has been split into two categories depending on the number of c-jets. The signal is scaled by a factor of 100 for visual clarity.

A comparison of the m_{vis} distribution of the signal in each channel is shown in Figure 4a where the distributions are normalised to the same number of events so that the resolution can be compared. From the figure it is seen how much better the resolution of the leptonic channels is in comparison to the hadronic ones. Based on the distributions shown in Figures 2 and 4a a requirement on m_{vis} is optimized to be in the range 88–94 GeV for the leptonic channels and 88–100 GeV in the hadronic channels to suppress WW, Z/γ^* and Higgs boson backgrounds.

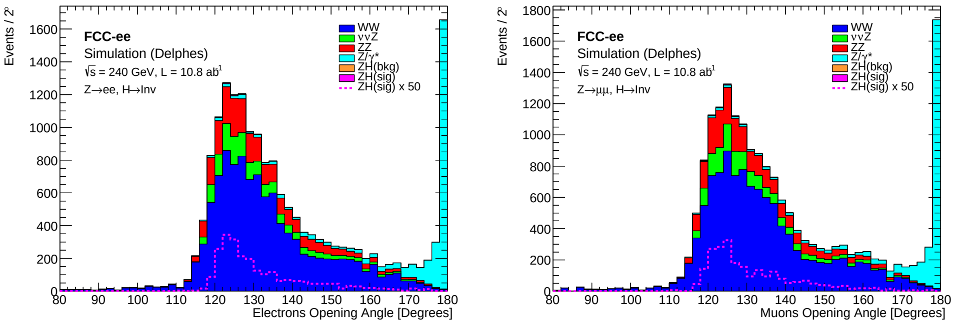

(a) (b)

Fig. 3: The opening angle between (a) electrons in ee channel and (b) muons in $\mu\mu$ channel in degrees for $\sqrt{s} = 240$ GeV after the m_{vis}, $p_{\text{T}}^{\text{miss}}$ requirement and the additional requirement of $120 < m_{\text{miss}} < 130$ GeV.

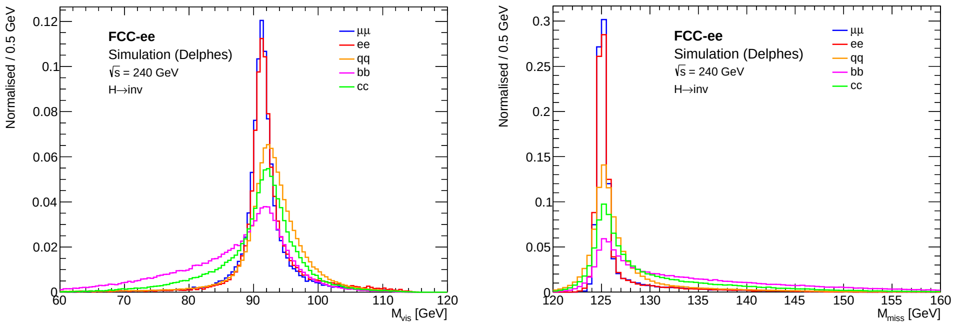

(a) (b)

Fig. 4: (a) The m_{vis} and (b) the m_{miss} distributions of the different channels for the signal samples. The distributions are normalised to the same number of events and have the $p_{\text{T}}^{\text{miss}}$ requirement.

To separate background processes where the decay particles are coming from different particles, an opening angle cut is used in the leptonic channel shown in Figure 3. The Z/γ^* background has a large opening angle due to the $Z \to \tau\tau$ process. Allowing a selection to be placed on both leptonic channels of the opening angle being less than 155° to remove the $Z \to \tau\tau$ background.

The final result is obtained using the m_{miss} distribution, which is shown in Figure 4b for the signal for the different channels after all selection requirements. The signal distributions are normalized to the same number of events so that the resolution can be compared. It is seen that the hadronic channels have worse resolution. In addition, the long tail towards higher m_{miss} in the bb and cc channels is observed, which

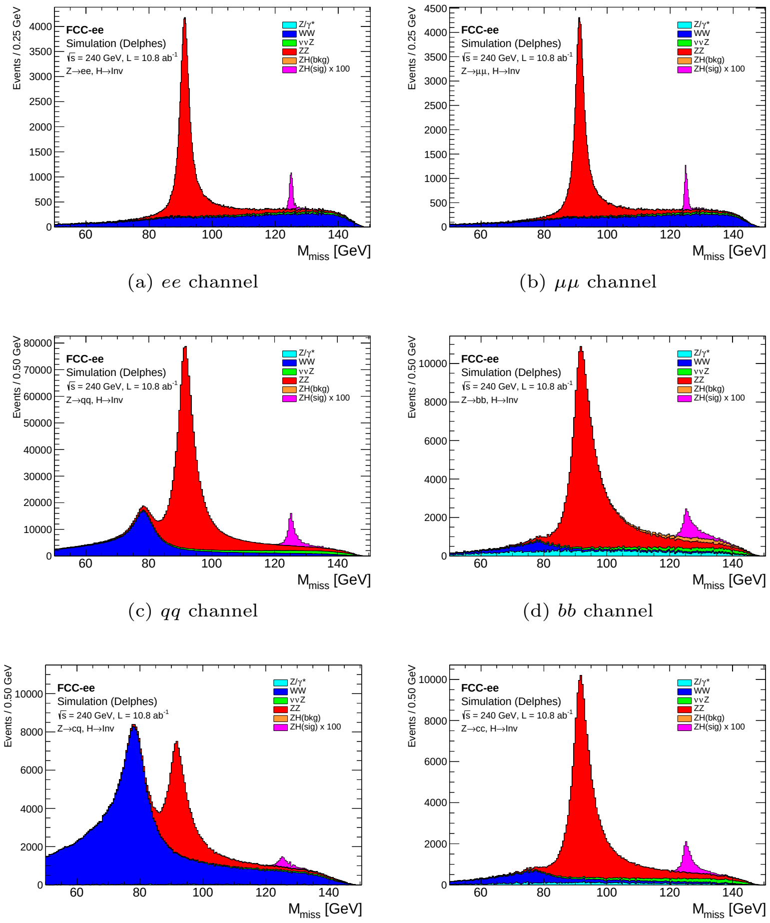

(a) ee channel

(b) $\mu\mu$ channel

(c) qq channel

(d) bb channel

(e) cc channel, 1 c-jet

(f) cc channel, 2 c-jets

Fig. 5: The m_{miss} distribution of (a) ee, (b) $\mu\mu$, (c) qq, (d) bb and (e-f) cc channels for $\sqrt{s} = 240$ GeV after all selection requirements. The cc channel has been split into two categories depending on the number of c-jets. The signal is scaled by a factor of 100 for visual clarity.

is due to neutrinos in the final state. The comparison of the m_{miss} distribution after the other selections for backgrounds and signal is shown in Figure 5. It can be seen that the signal is well separated from the majority of the ZZ background but there is still a large background in many of the channels due to non-resonant production. The WW background is dominant in the leptonic and 1 c-jet cc channels, whereas Z production is only a significant background in the bb and cc channels. Background from Higgs production with different decays to the signal is very small in all channels.

4 Analysis at $\sqrt{s} = 365$ GeV

The Analysis at $\sqrt{s} = 365$ GeV follows closely that at $\sqrt{s} = 240$ GeV presented in Section 3. However, there are some important differences: the larger $\sqrt{s}$ means the average energy of the final state particles increases; top pair production is present; and vector-boson fusion processes such as $ee \to WW\nu\nu \to ZZ\nu\nu$ and $ee \to WW\nu\nu \to Z\nu\nu$ become larger when running at the higher $\sqrt{s}$ value. These effects cause an overall relative increase in background compared with signal.

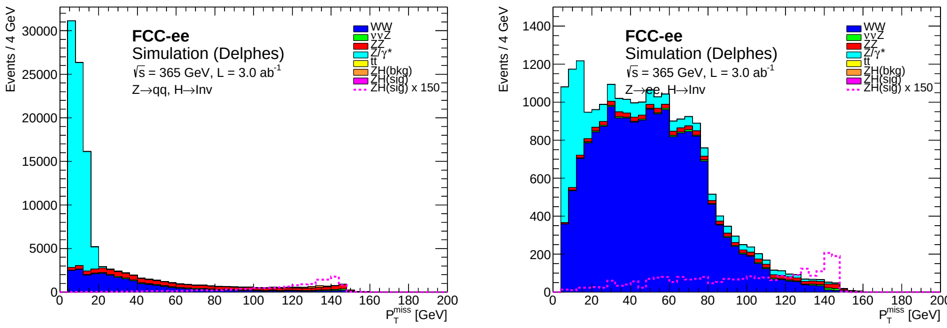

(a) qq channel (b) ee channel

Fig. 6: The missing p_T distribution of (a) qq and (b) bb channels for $\sqrt{s} = 365$ GeV after the m_Z selection requirements. For visual clarity events with $p_{\mathrm{T}}^{\mathrm{miss}} < 5$ GeV are removed and the signal is scaled by a factor of 100.

A minimum $p_{\mathrm{T}}^{\mathrm{miss}}$of 60 GeV for the ee and $\mu\mu$ channels and 100 GeV for the qq, cc and bb channels helps reduce WW and ZZ background as well as $Z\gamma^*$ backgrounds as can be seen in Fig.6 where two example channels are shown. Figure 7 shows the m_{vis} distribution for all Z decay channels explored in this analysis. It can be seen that the signal extends to larger values than at $\sqrt{s} = 240$ GeV due to increased initial state photon radiation, necessitating an increase range for the selection of $88 < m_{\mathrm{vis}} < 130$ GeV. The extra energy collision affects the opening angle of the particles with a decrease for particles which come from the same particle decay shown in Figure 8. This allows to better separate the WW and remove the $Z \to \tau\tau$ background with a selection of the opening angle being less than 125°.

The comparison of the m_{miss} distribution after the other selections for backgrounds and signal is shown in Figure 9. The signal resolution is worse for the hadronic channels than at $\sqrt{s} = 240$ GeV. As at the lower beam energy the WW background is dominant in the leptonic and 1 c-jet cc channels, whereas $Z\gamma^*$ production is only a significant background in the bb and cc channels.

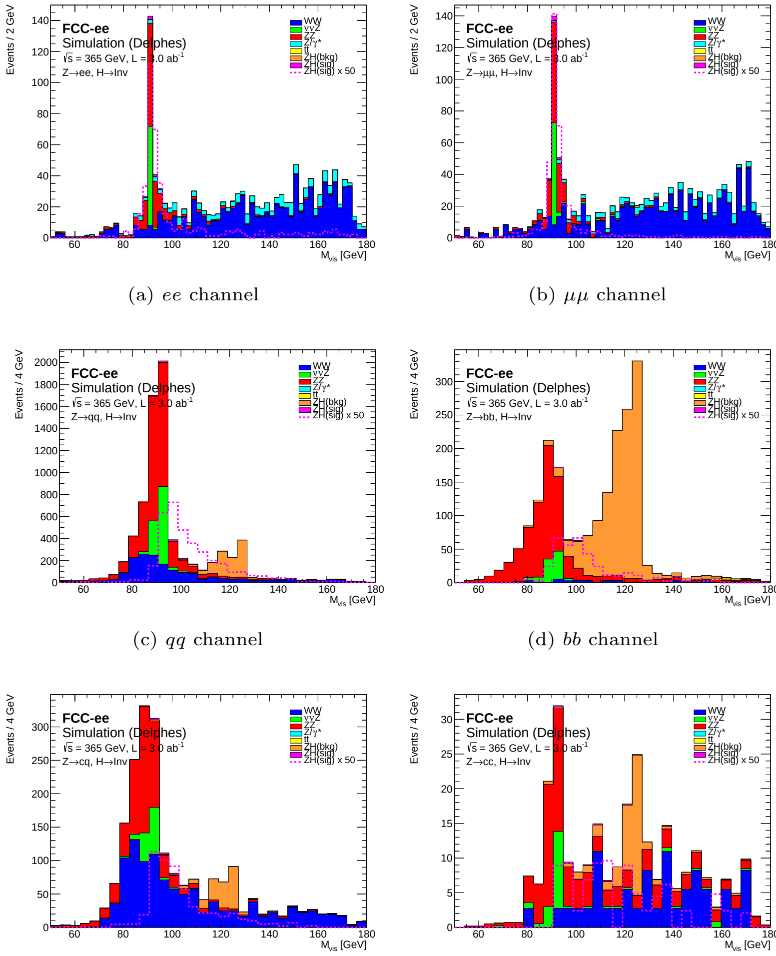

(a) ee channel

(b) $\mu\mu$ channel

(c) qq channel

(d) bb channel

(e) cc channel, 1 c-jet

(f) cc channel, 2 c-jets

Fig. 7: The m_{vis} distribution of (a) ee, (b) $\mu\mu$, (c) qq, (d) bb and (e-f) cc channels for $\sqrt{s} = 365$ GeV after the $p_{\text{T}}^{\text{miss}}$ requirement and the additional requirement of $120 < m_{\text{miss}} < 130$ GeV. The cc channel has been split into two categories depending on the number of c-jets. The signal is scaled by a factor of 100 for visual clarity.

5 Results

The final result is obtained by a likelihood fit of the m_{miss} distributions in each category, shown in Figures 5 using the software package `HistFitter` [2]. The signal is floated, along with the ZZ and WW backgrounds. Smaller backgrounds from ZH,

[2]`https://histfitter.github.io/`

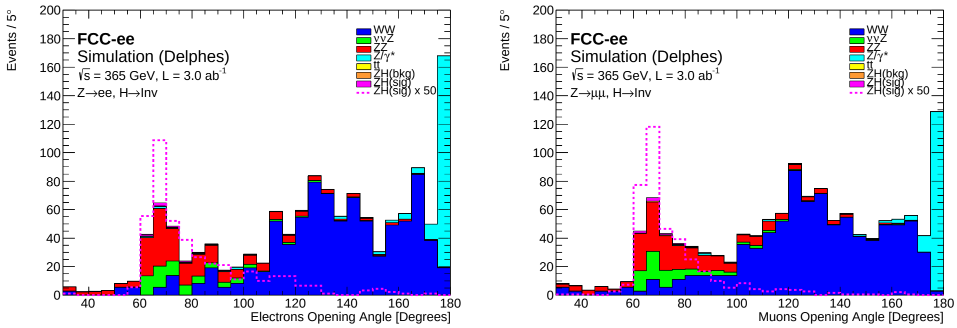

(a) (b)

Fig. 8: The Opening Angle between (a) electrons in ee channel and (b) muons in $\mu\mu$ channel in degrees for $\sqrt{s}$ = 365 GeV after the m_{vis}, $p_{\mathrm{T}}^{\mathrm{miss}}$ requirement and the additional requirement of $120 < m_{\mathrm{miss}} < 130$ GeV.

which includes Higgs boson decays that do not decay to invisible, as well as dilepton backgrounds are kept fixed to their predicted cross sections. The model for signal and background is fitted against an Asimov dataset [14] for the extraction of the final result. Upper limits that are quoted in the follow are calculated using the modified frequentist approach that is discussed in Ref. [15].

The results are quoted without including systematic errors, but since the backgrounds are all non-resonant and can be well constrained from the side-bands it is not thought that systematic uncertainties will affect the results appreciably. It should be noted that the results are very dependent on the resolution though and could be degraded if the actual detector configuration or reconstruction algorithms do not perform as well as in the Monte Carlo simulation presented here.

There are fits that are performed for two separate scenarios. The first fit aims to estimate the sensitivity in measuring the SM Higgs boson to invisible branching ratio. In this fit, the SM Higgs boson to invisible signal is floated. The signal and background prediction is fitted against an Asimov dataset in which the SM Higgs boson to invisible signal is fixed to the SM expectation. The result is expressed in terms of a 68% confidence level interval on the Higgs boson to invisible branching ratio and it is shown for each channel separately, as well as for the combination of all channels in Figure 10. Also shown in this figure are the results obtained from the data at the two beam energies and the combined result. It can be seen that the qq channel is the most sensitive and results at $\sqrt{s}$ = 240 GeV are much better than those from $\sqrt{s}$ = 365 GeV, as was expected from the lower integrated luminosity and signal cross section at the higher beam energy. The combination of all channels and both beam energies would correspond to a measurement with a 0.027% uncertainty, which corresponds to an observation with significance of 3.9σ.

A different scenario assumes the SM Higgs boson to neutrinos as a background and searches for a Higgs boson to invisible particles that are beyond the SM. The fit is

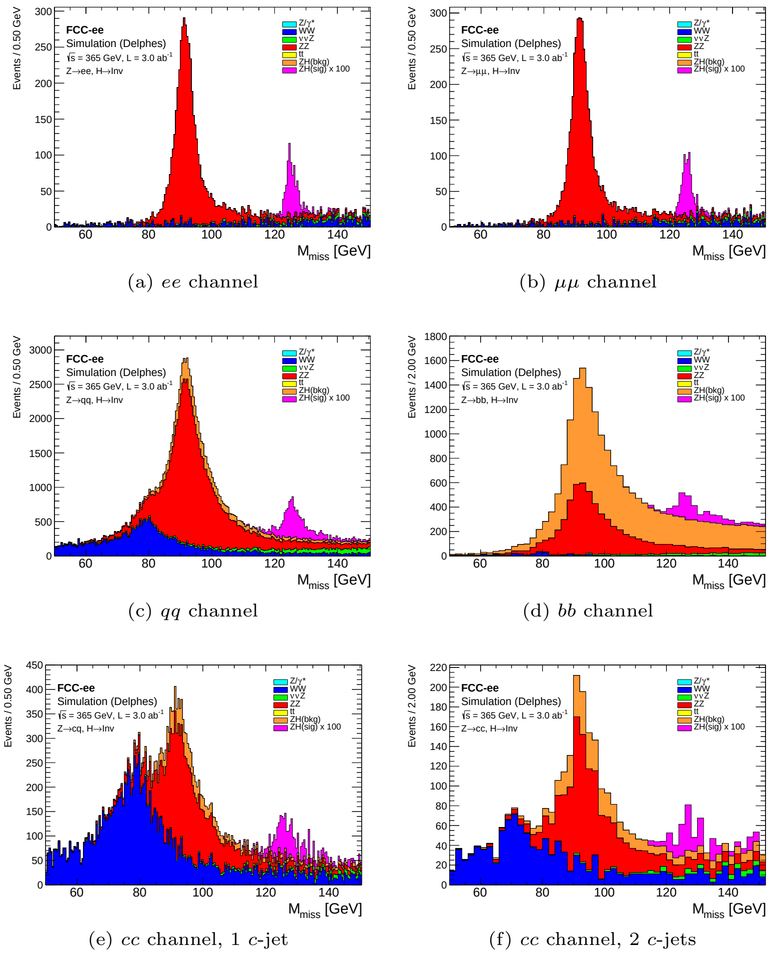

(a) ee channel

(b) $\mu\mu$ channel

(c) qq channel

(d) bb channel

(e) cc channel, 1 c-jet

(f) cc channel, 2 c-jets

Fig. 9: The m_{miss} distribution of (a) ee, (b) $\mu\mu$, (c) qq, (d) bb and (e-f) cc channels after all selection requirements for $\sqrt{s} = 365$ GeV. The cc channel has been split into two categories depending on the number of c-jets. The signal is scaled by a factor of 100 for visual clarity.

performed then to estimate the smallest branching fraction of such a beyond SM process that would lead to a 5 σ discovery and the results are shown in Figure 11a where the results from a combination of the data from both beam energies is shown. Again, the qq channel is the most sensitive and the combination of all channels indicates that if the Higgs boson to invisible beyond SM particles is 0.13% or above a 5-σ discovery is expected. In case of no discovery, 95% confidence level upper limits are derived for each of channels and their combination, as shown in Figure 11b. The expectation for the sensitivity is that branching fractions of Higgs boson to invisible beyond SM

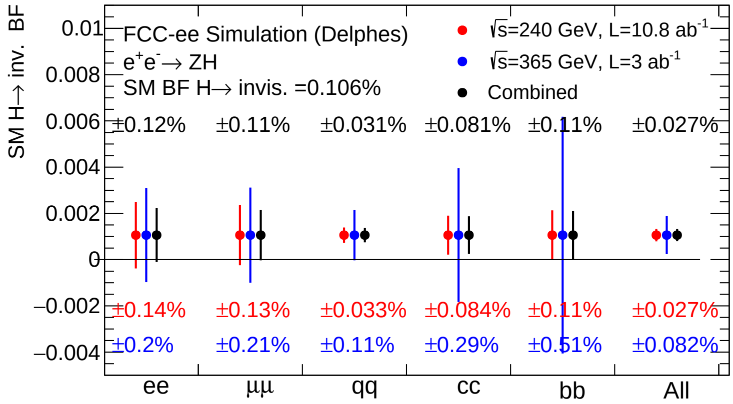

Fig. 10: The expected uncertainty on a measurement of the branching fraction of Higgs boson to invisible particles for the individual channels and all channels combined. Results shown are for the data at $\sqrt{s} = 240$ GeV and $\sqrt{s} = 365$ GeV and at the two beam energies combined. The branching fraction of Higgs boson to invisible particles is set to the SM value for $H \to ZZ \to \nu\nu\nu\nu$ of 0.106%.

particles larger than 0.052% will be excluded at 95% confidence level. The individual limits are 0.055% and 0.16% for $\sqrt{s} = 240$ GeV and $\sqrt{s} = 365$ GeV respectively.

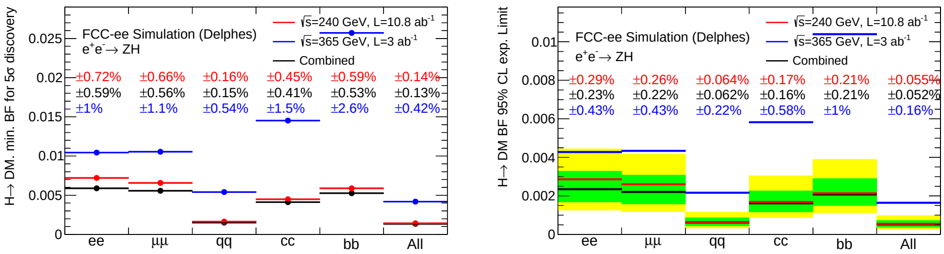

(a) (b)

Fig. 11: (a) The minimum for a 5σ discovery and (b) the limit at 95% confidence level on the branching fraction of the Higgs boson to new invisible particles for the individual channels and all channels combined. Results shown are for the data at $\sqrt{s} = 240$ GeV and $\sqrt{s} = 365$ GeV and at the two beam energies combined. The contribution from SM Higgs boson to neutrinos is treated as a background.

6 Resolution Studies

The effects of a poorer detector energy resolution on the measurement is investigated by applying a simple additional Gaussian smearing either to the four vector of the hadronic final state as shown in Figure 12 (a) or to the leptons as shown in Figure 12 (b). These studies were performed for an integrated luminosity of 5 ab^{-1} at $\sqrt{s} = 240$ GeV. It can be seen that an additional hadronic smearing has a significant effect on the qq channel, with a 130% increase in the error for a 5% additional smearing. However, in the combination the error increase is reduced to 80% due to the leptonic channels which do not suffer in this scenario. Conversely, if the leptonic resolution were worse than expected this would have a limited effect on the combined measurement with an 8% increase in error for a 5% additional leptonic energy smearing.

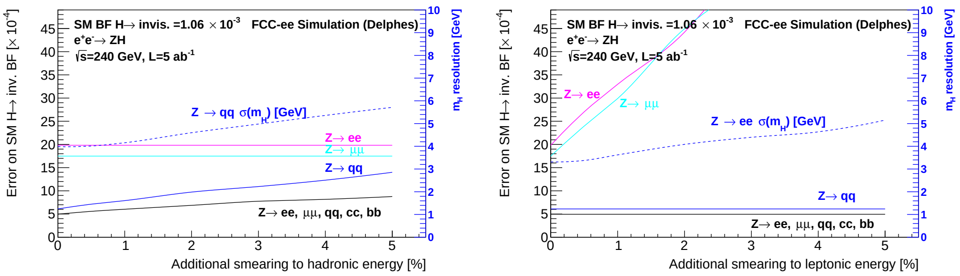

(a) (b)

Fig. 12: The effect of an addition smearing to the (a) hadronic energy and (b) leptonic energy. The expected uncertainty on a measurement of the branching fraction of Higgs boson to invisible particles for selected individual channels and all channels combined is shown. In addition the root mean squared of the reconstructed Higgs mass is also shown.

7 Conclusions

The expected sensitivity to the branching fraction of $H \to$ invisible is estimated for the ZH process at the Future Circular Collider running with a total integrated luminosity of 10.8 ab^{-1} at $\sqrt{s} = 240$ GeV and 3 ab^{-1} at $\sqrt{s} = 365$ GeV. The decay of the Z to electrons, muons, b-quarks, c-quarks and lighter quarks was investigated. It is found that a 25% measurement is possible if a Standard Model branching fraction of 0.106% is assumed. The $Z \to qq$ channel has the best sensitivity and the $\sqrt{s} = 240$ GeV run has much better sensitivity than the one at $\sqrt{s} = 365$ GeV. Additional new physics $H \to$ invisible decays could be observed with a significance of more than 5σ if the branching fraction exceeds 0.13% or could be excluded at 0.052% at the 95% confidence level. Although systematic uncertainties were not included in this study they are not thought likely to appreciably change the results.

References

[1] A. Abada, et al., FCC Physics Opportunities: Future Circular Collider Conceptual Design Report Volume 1. Eur. Phys. J. C **79**(6), 474 (2019). https://doi.org/10.1140/epjc/s10052-019-6904-3

[2] D. de Florian, et al., Handbook of LHC Higgs Cross Sections: 4. Deciphering the Nature of the Higgs Sector **2/2017** (2016). https://doi.org/10.23731/CYRM-2017-002. arXiv:1610.07922 [hep-ph]

[3] B. Patt, F. Wilczek, Higgs-field portal into hidden sectors (2006). arXiv:hep-ph/0605188

[4] S. Argyropoulos, O. Brandt, U. Haisch, Collider Searches for Dark Matter through the Higgs Lens. Symmetry **13**(12), 2406 (2021). https://doi.org/10.3390/sym13122406. arXiv:2109.13597 [hep-ph]

[5] Combination of searches for invisible decays of the Higgs boson using 139 fb^{-1} of proton-proton collision data at $\sqrt{s}$ = 13 TeV collected with the ATLAS experiment (2023). arXiv:2301.10731 [hep-ex]

[6] A search for decays of the Higgs boson to invisible particles in events with a top-antitop quark pair or a vector boson in proton-proton collisions at $\sqrt{s}$ = 13 TeV (2023). arXiv:2303.01214 [hep-ex]

[7] Y. Tan, et al., Search for invisible decays of the Higgs boson produced at the CEPC. Chin. Phys. C **44**(12), 123001 (2020). https://doi.org/10.1088/1674-1137/abb4d8. arXiv:2001.05912 [hep-ex]

[8] O. Cerri, M. de Gruttola, M. Pierini, A. Podo, G. Rolandi, Study the effect of beam energy spread and detector resolution on the search for Higgs boson decays to invisible particles at a future $e^+ e^-$ circular collider. Eur. Phys. J. C **77**(2), 116 (2017). https://doi.org/10.1140/epjc/s10052-017-4680-5. arXiv:1605.00100 [hep-ex]

[9] T.I.S. Group. The idea detector concept for fcc-ee (2025). URL https://arxiv.org/abs/2502.21223

[10] J. de Favereau, C. Delaere, P. Demin, A. Giammanco, V. Lemaître, A. Mertens, M. Selvaggi, DELPHES 3, A modular framework for fast simulation of a generic collider experiment. JHEP **02**, 057 (2014). https://doi.org/10.1007/JHEP02(2014)057. arXiv:1307.6346 [hep-ex]

[11] M. Cacciari, G.P. Salam, G. Soyez, FastJet User Manual. Eur. Phys. J. C **72**, 1896 (2012). https://doi.org/10.1140/epjc/s10052-012-1896-2. arXiv:1111.6097 [hep-ph]

[12] H. Qu, L. Gouskos, ParticleNet: Jet Tagging via Particle Clouds. Phys. Rev. D **101**(5), 056019 (2020). https://doi.org/10.1103/PhysRevD.101.056019. arXiv:1902.08570 [hep-ph]

[13] F. Bedeschi, L. Gouskos, M. Selvaggi, Jet flavour tagging for future colliders with fast simulation. Eur. Phys. J. C **82**(7), 646 (2022). https://doi.org/10.1140/epjc/s10052-022-10609-1. arXiv:2202.03285 [hep-ex]

[14] G. Cowan, K. Cranmer, E. Gross, O. Vitells, Asymptotic formulae for likelihood-based tests of new physics. Eur. Phys. J. C **71**, 1554 (2011). https://doi.org/10.1140/epjc/s10052-011-1554-0. [Erratum: Eur.Phys.J.C 73, 2501 (2013)]. arXiv:1007.1727 [physics.data-an]

[15] A.L. Read, Presentation of search results: The CL(s) technique. J. Phys. G **28**, 2693–2704 (2002). https://doi.org/10.1088/0954-3899/28/10/313